Impact of horizontal resolution on simulation of precipitation extremes in an aqua-planet version of Community Atmospheric Model (CAM3)

Fuyu Li[1*], William D. Collins[1], Michael F. Wehner[1], David L. Williamson[2], Jerry G. Olson[2], Christopher Algieri[1]

1. Lawrence Berkeley National Laboratory, 1 Cyclotron Road, MS 50A4037, Berkeley, CA 94720, USA;

2. National Center for Atmospheric Research, Boulder, CO, USA

[*] Corresponding author.
Email: fli@lbl.gov

Abstract

One key question regarding current climate models is whether the projection of climate extremes converges to a realistic representation as the spatial and temporal resolutions of the model are increased. Ideally the model extreme statistics should approach a fixed distribution once the resolutions are commensurate with the characteristic length and time scales of the processes governing the formation of the extreme phenomena of interest. In the current study, a series of AGCM runs with idealized "aquaplanet-steady-state" boundary conditions have been performed with the Community Atmosphere Model CAM3 to investigate the effect of horizontal resolution on climate extreme simulations. The use of the aquaplanet framework highlights the roles of model physics and dynamics and removes any apparent convergence in extreme statistics due to better resolution of surface boundary conditions and other external inputs. Assessed at a same large spatial scale, the results show that the horizontal resolution and time step have strong effects on the simulations of precipitation extremes. The horizontal resolution has a much stronger impact on precipitation extremes than on mean precipitation. Updrafts are strongly correlated with extreme precipitation at tropics at all the resolutions, while positive low-tropospheric temperature anomalies are associated with extreme precipitation at mid-latitudes.

1. Introduction

Changes in extreme weather events could represent some of the most important consequences of the climate change, since these events can seriously affect both human society and the natural environment. Extreme phenomena pose particular dangers to society, in particular because developing countries may not necessarily be prepared for the consequences of intense and episodic meteorological conditions (Parry et al., 2007). Along with the warming of climate in recent decades, significant trends in the magnitude, frequency, and geographical distributions of some weather extremes have been observed (Schneider and O'Gorman, 2007; Trenberth et al., 2007).

The current generation of climate models, however, is based upon earlier generations historically designed to produce realistic mean climate statistics. The capacity of these models to simulate the statistics of rare weather events is therefore an open question at present, and in fact climate models may not reproduce the physical mechanisms that cause extreme weather events (Sun et al, 2006). While extreme precipitation is a particularly important hydrometeorological phenomenon, moist convective parameterizations are not necessarily designed to capture high-order statistics of rainfall. Wilcox and Donner (2007) found that simulations using two different convection schemes resulted in greater changes in the frequency of precipitation extremes than the changes due to 2-degree surface warming using either scheme. The IPCC assessments (Randall et al., 2007) have suggested that there are inconsistencies for future projections of hydrological extremes across the climate models, with significant differences across the IPCC multi-model ensemble.

Two key issues for modeling extremes are the effects of horizontal resolution on these phenomena and hence the fidelity of simulations using ultra-high-resolution model grids. Many types of extremes, for example downpours and cyclones, are inherently highly localized in space and time. A critical requirement for robust projection of these phenomena is that the simulated extreme statistics converge as the model grid resolution approaches or exceeds the characteristic length and time scales for the phenomena of interest. While the higher-resolution simulations, by default, add finer scales into the simulation results, these integrations, when averaged to coarser scales, do not necessarily produce the same climatological distributions of extremes as coarser resolution runs. In this study, we consider the simulation to have converged if the larger scales are not affected by the addition of smaller scales in the model and the increasing horizontal resolution simply adds finer scales to the simulations (Williamson, 2008).

Boyle and Klein (2010) reported that increasing horizontal resolution appears to improve the precipitation intensity statistics, but the distributions from different resolution runs do not agree with each other even when the precipitation has been interpolated to the coarser grid before calculating the statistics. Although high resolution models, specifically a 0.5° mesh or finer, have been suggested to be essential for accurate simulation of rainfall extreme events in the historical climate record (e.g. Chen and Knutson 2008; Wehner et al. 2010), these models also exhibited large precipitation errors by accentuating errors apparent at low resolutions (Pope and Stratton, 2002; Lau and Ploshay, 2009). It is therefore important to know if the simulations on extremes would converge with increasing resolution even under the simplest model configuration.

This study will address the above issues and investigate the robustness of climate models in simulating hydrological extremes. We use atmospheric stand-alone simulations with highly simplified and idealized surface boundary conditions to test if the extreme simulations converge across resolution. Heterogeneities in the land surface can affect the transfer of momentum, heat, and water between the land and atmosphere through highly nonlinear processes (Giorgi and Avissar, 1997), and there are significant coupled synoptic-scale responses to sub-mesoscale land-surface features (Ghan et al. 2002). For these reasons, we adopt the aqua-planet configuration for our runs (Neale and Hoskins, 2000) in which the entire planetary surface is treated as an ocean with specified zonally symmetric sea-surface temperatures (SST). The absence of variations in underlying surface types and orography under the aqua-planet framework means that the surface boundary condition and its influence on the atmosphere are held constant under varying resolutions. The elimination of resolution-dependent signals from the boundary conditions should help isolate the mechanisms driving the rainfall extremes in the free atmosphere. Similar frameworks have been used to investigate rainfall extremes and the corresponding errors in current climate models (e.g. O'Gorman and Schneider, 2009). The use of stand-alone atmospheric models inherent in the aquaplanet configuration excludes signals from the improvements observed in ocean and ocean-atmosphere simulations with increased horizontal resolutions. By this means, we focus on the convergence due solely to atmospheric climate models' parameterizations and dynamics. The details of the model are described in section 2. The results of the simulations are shown in Section 3, and we present the conclusions in section 4.

2. Model description

We set up a series of idealized AGCM runs using the NCAR Community Atmospheric Model Version 3.0 (CAM3) at different resolutions (Collins et al., 2004). These simulations are configured using the "aquaplanet-steady-state" boundary conditions (Neale and Hoskins, 2000), similar to previous work conducted by Williamson (2008).

The simulations employ the CAM Eulerian spectral transform dynamic core. Ten experiments are performed at four horizontal resolutions corresponding to spectral truncations of T42, T85, T170, and T340 (~2.8°, 1.4°, 0.7°, and 0.35° transform grids, respectively), and at different parameterization time steps (40, 20, 10 and 5 minutes) at or below their nominally dynamically stable values at each resolution. The vertical resolution is 26-level vertical grid of standard CAM3 configuration. With one minor exception, all the experiments use the same set of the adjustable parameters in the physics suite as the standard values used by default for the T85 resolution (Collins et al, 2004). The exception is that the ∇^4 diffusion coefficients in the prognostic equations for temperature, divergence and vorticity introduced to provide reasonable kinetic energy spectra are set to 1.0 $x10^{16}$, $1.0x10^{15}$, $1.5x10^{14}$, and $1.5x10^{13}$ m^4 s^{-1} for T42, T85, T170 and T340 runs, respectively.

The CAM3 is run in stand-alone mode with a prescribed SST distribution following the aquaplanet control experiment protocol described by Neale and Hoskins (2000). Diurnally cyclic insolation is imposed under fixed equinoctial conditions and is therefore symmetric about the equator. There are no radiatively active aerosols and the only radiatively active gases are well mixed greenhouse species set to current concentrations. They are symmeterized about the equator and in the zonal direction. The

aerosol specification for cloud condensation is set to a time-invariant distribution appropriate for oceanic conditions and is also symmetric about the equator and in the zonal direction. It follows from the zonally symmetric boundary conditions at the surface and the top of the model atmosphere that the statistics of the simulation climate are also zonally symmetric. We exploit this zonal symmetry to identify statistically significant zonal-mean signals using only relatively short integrations of CAM.

The simulations start from a state taken from a previous aqua-planet simulation, and we treat the first year as the "spin up" period in our runs. In fact, the model transitions from its initial conditions to its aqua-planet climate in less than 2 months (Williamson, 2008). The simulation periods are 16, 8, 4, and 2 years for T42, T85, T170, and T340 respectively. The inverse relationship between spatial resolution and simulation period follows from the statistical convergence afforded by zonal symmetry and by the doubling of the number of grid points in the zonal direction with each refinement in resolution. The sampling sizes are sufficient to maintain the simulation errors below desirable levels for most of the extreme events (e.g. the 99^{th} percentile precipitation or 10-year return value) at the model original grids. For the "convergence" issue targeted in this study, we primarily use the 95^{th} percentile extreme precipitation (detailed before) and average the absolute values to 5-degree coarser grid before calculating precipitation extremes, for all the figures below through conservative remapping as suggested by (Chen and Knutson, 2008). Two years are the minimum integration period needed for enough samples to get the statistical error below ~10% (95% confidence level) for the extreme precipitation on the 5-degree grid. Under the aqua-planet configuration, the inter-annual variability for the low-resolution simulations is actually very small and there

are no large statistically differences between a two-year simulation and longer simulations. The long simulation periods for the low-resolution experiments are designed to maintain the simulation errors below desirable levels for most of the extreme events (e.g. the 99th percentile precipitation or 10-year return value) at the model original grids.

In this paper, we focus on the hydrological extremes based on commonly used measures of weather extreme known as Frich indices (Frich et al., 2002; Alexander et al. 2006). The extreme precipitation used in this study is the annual total 95th percentile wet-day precipitation (here after: R95pTOT). R95pTOT is a commonly used index for extreme precipitation (e.g. Christensen and Christensen, 2003; Alexander et al., 2006) and is calculated by summing over an annual cycle all the daily precipitation larger than the 95th percentile of the climatological daily precipitation in wet-days:

$$\mathrm{R95pTOT} = \sum_{i=1}^{W} \mathrm{prec}_i \quad \text{when} \quad \mathrm{prec}_i > \mathrm{p95} \tag{1}$$

where $prec_i$ is the daily precipitation on a wet day i (when daily precipitation > 1 mm/day), W is the total number of wet days, and $p95$ is the 95th percentile of wet-day precipitation in the year.

3. Results

The time-averaged, zonal-averaged daily total precipitation and the R95pTOT precipitation extremes for all the ten experiments are shown in Figure 1. The precipitation has been averaged to a 5° grid (87.5°S - 87.5°N), before calculating precipitation

extremes, with a mass-conserving interpolation method to eliminate the effect from adding finer scales in the higher resolution simulations. The precipitation extremes have been calculated from the spatially averaged precipitation. In fact, all analyses in this paper are based on similarly averaged data. Figures 1a-1i show the relative difference of the precipitation and precipitation extremes for T42, T85, and T170 and a range of physics time steps, relative to the corresponding fields from a T340 simulation with a 5-minute time step (Figure 1j). These results indicate the degree of convergence of these fields across horizontal scales and time steps, i.e. whether the larger scales are affected by the addition of smaller scales in the model. In Figure 1, some combinations of longer time steps and higher resolutions are omitted if the dynamic core would be computationally unstable according to the Courant–Friedrichs–Lewy (CFL) condition (Courant et al., 1967).

There are local maxima for both mean and extreme precipitation near the equator and at mid-latitude regions analogous to the Intertropical Convergence Zone (ITCZ) and storm tracks of the real climate system (Figure 1j). The daily mean precipitation generally increases with increasing horizontal resolution and decreasing time steps as shown by Williamson (2008) for the same model. The increase in mean precipitation is more dramatic for the GCM simulations performed in the standard mode with time steps that decrease with increasing resolution in accordance with the CFL criterion. These simulations are plotted along the outer diagonal in Figure 1 (panels a, e, h, and j). Most atmospheric models used for climate projection in, for example, the Second and Third Assessment Reports (SAR and TAR) of the IPCC have had grids comparable to T42 resolution. The mean and extreme precipitation in the T42 simulation are significantly

smaller than the corresponding fields in the T340 simulation for most latitudes. In the equatorial band, the mean precipitation is ~20% and the extreme precipitation is ~70% lower than the corresponding fields in the T340 aqua-planet simulation (Figure 1a). Therefore, the simulation of precipitation extremes depends on the horizontal and temporal resolutions used for the climate models, even for these larger scales present in the 5-degree grid.

Figure 1 also shows that the horizontal resolution has a stronger impact on precipitation extremes than mean precipitation. For instance, the mean precipitation projected onto a 5-degree grid shows some signs of convergence at the equator across different resolutions run with the same time step. This is evident in results with a 20 minute time step (Figure 1b, 1e), 10 minute time step (Figure 1c, 1f, 1h), and 5 minute time step (Figure 1d, 1g, 1i, and 1j). However, the differences of corresponding precipitation extremes are much larger, and the extremes do not to converge with increasing resolution, except for that at T170 with a 5 minute time step (Figure 1i). These differences suggest that the statistics of precipitation and precipitation extremes could be sensitive to different mechanisms. Therefore the rate of improvement in the mean precipitation with increased resolution need not apply to extreme precipitation. Other differences in mean and extreme precipitation have been observed in previous climate simulations. Pall et al. (2007), for example, have shown that precipitation extremes increased faster than mean precipitation in response to global warming.

In CAM3, the total precipitation in the model is parameterized as a sum of contributions from various sources and processes. One can also examine which precipitation components contribute to the divergence of precipitation extremes as a

function of resolution. In an ideal scale-invariant representation, the relative contributions to the total rainfall rates would be insensitive to resolution. The total precipitation consists of two major components: convective precipitation (denoted by PRECC below) and large-scale precipitation (PRECL). In CAM3, the convective precipitation in turn is treated as the sum of two separate processes: deep convection (denoted by PREC_zmc) and shallow/middle tropospheric convection (PREC_cmf). The large-scale precipitation is also treated by a combination of two processes: prognostic precipitation (PREC_pcw) and cloud sedimentation (PREC_sed). More details of the CAM3 precipitation parameterization are described in Collins et al. (2004), and the fidelity of the resulting distributions and types of hydrometeors are described in Rasch et al. (2006). The daily precipitation during extreme events resolved into these components is shown in Figure 2. The precipitation from shallow/middle tropospheric convection (PREC_cmf) and cloud sedimentation (PREC_sed) are not shown in the figure, since the magnitudes of these components are much less than those from deep convection (PREC_zmc) and prognostic precipitation (PREC_pcw). Rasch et al (2006) show that the relative amounts of convective and stratiform precipitation differ markedly from retrievals of these amounts from the Tropical Rainfall Mapping Mission (TRMM) in CAM simulations run with T85 resolution. Therefore the correspondence of the total precipitation to various observational estimates in those simulations derives from compensating errors between the two sets of processes. It should be noted that most convective and stratiform processes in the tropics are still subgrid at typical climate models' resolutions, and are related to subgrid convective dynamics. The separation of large-scale and convective

parameterizations in the climate model may be quite arbitrary compared with the actual stratiform and convective precipitation.

The tropical mean precipitation results primarily from sub-grid convection in the experiments with low resolutions and longer time steps (not shown here). However in the extratropics, it is a mixture of resolved grid-scale condensation and sub-grid convection (also not shown here). This feature changes significantly during extreme events as large-scale precipitation becomes much more dominant (Figure 2). In simulations at T42 resolution, the convective precipitation is slightly higher than the large-scale precipitation in the tropics and sub-tropics. For all the other higher resolution experiments, the large-scale precipitation dominates at almost all the latitudes. This component of the precipitation originates almost entirely from the prognostic precipitation, while the convective precipitation mostly comes from deep convection (PREC-zmc).

The total extreme precipitation at the equator and mid-latitudes increases with increasing horizontal resolution from T42 to T170, and decreases slightly at T340 (black line in Figure2). This was already seen in Figure 1. The convective precipitation decreases, while large-scale precipitation increases, with increasing horizontal resolution similar to the trends found in previous studies (Duffy et al. 2003; Boyle and Klein 2010). The opposite trends indicate that the two types of precipitation are due to different mechanisms. While simple mechanisms that account for the effects of adiabatic lapse rate, circulation strength, and temperatures could explain the meridional distributions of both types of precipitation in low resolution idealized GCMs (O'Gorman and Schneider, 2009), additional considerations are required for higher resolutions.

The trend in total extreme precipitation with resolution has the same sign as that of the corresponding large-scale precipitation, but it has the opposite sign to that of its convective precipitation component. The parameterization of prognostic large-scale precipitation seems to contribute to most of the differences, and the increasing resolution results in a shift of the probability distribution of daily precipitation. Kharin et al. (2007) noted large discrepancies in the changes in tropical precipitation extremes in their present-day simulations across the multi-model ensemble assembled for IPCC AR4. Most previous work attributes the discrepancy in the tropics to the sub-grid parameterizations of deep convection. However, as we show in Figure 2, the sensitivity of the extreme precipitation to horizontal resolution is also large in the tropics where the prognostic large-scale precipitation has a stronger sensitivity to horizontal resolution than does the convective precipitation.

The difference between mean precipitation and extreme precipitation is indicative of a change of the precipitation intensity across horizontal resolutions. Boyle and Klein (2010) have reported that increasing horizontal resolution appears to improve the statistics of precipitation intensity through coincident increases in the frequency of very high and very low precipitation rates. Here we specifically look into the equatorial regions (5° S – 5° N) where there is strong dependence on resolution. Figure 3 shows the probability distribution for total precipitation (PRECT), convective precipitation (PRECC), and large-scale precipitation (PRECL). The equatorial total precipitation starts to diverge at 20 mm/day. The probability for high precipitation increases from T42 to T170 but decreases slightly at T340, and the decrease from T170 to T340 is partially due to the spatial averaging before calculating the extremes (the precipitation increases from

T170 to T340 at their original grids). While the higher resolution runs show signs of convergence (for the daily precipitation less than 80mm/day in Figure 3), the T42 simulation significant underestimates the probabilities of high precipitation rates compared with those obtained at greater resolutions. The convective precipitation (PRECC) in tropics does not appear to diverge and rarely produces any precipitation greater than 30 mm/day on the 5° grid for any resolution, partially due to the averaging. It is the main process contributing to low rates of precipitation (less than 10 mm/day), but the distribution of heavy tropical precipitation is primarily due to large-scale precipitation. It should be noted that the dominance of large-scale precipitation over convective precipitation at high rainfall rates is completely counter to observations (Schumacher and Houze, 2003). The impact of horizontal resolution on precipitation extremes is manifested primarily by its effects on large-scale precipitation. This is a counter-intuitive finding since convective precipitation is supposed to be more sensitive to model resolution due to its dependence on sub-grid convective processes. Hack et al. (2006) pointed out that this could result from the improved large-scale circulation at higher resolution.

Extreme precipitation is associated with strong convergence of horizontal fluxes. It may not necessarily scale with the atmospheric water content, since the strength of circulations varies and the atmosphere is not necessarily dried out during extreme events (O'Gorman and Schneider, 2009). Systematic fluctuations in the updraft velocity (measured using the large-scale vertical velocity as a proxy) and the surface temperature have been reported to be coupled with the occurrence of precipitation extremes (O'Gorman and Schneider, 2009). These fluctuations respectively represent the

"dynamic" and "thermodynamic" components of the drivers for extreme precipitation (Emori and Brown, 2005). Hence the anomalies of extreme precipitation (R95pTOT), vertical velocity ω, and temperature during the extreme events with respect to their mean values provide useful information for understanding the physical mechanisms for extreme precipitation. In this analysis, we choose the vertical velocity and temperature at 850 hPa level, to focus more on the low-tropospheric heating, which is the main driver for the convection. Additional tests showed that the correlations between extreme precipitation and vertical velocity (temperature) at 850 hPa and 500 hPa are very close.

Figure 4 shows that the anomalies in 850 hPa temperature during extreme events are vanishingly small in the tropics. There is no local warming at this level even due to the latent heat release from extreme precipitation because the maximum latent heating would likely appear near 500-600 hPa level over tropics (Boyle and Klein, 2010). In mid to high latitudes, the extreme events are usually accompanied by near-surface warming with positive temperature anomalies of between 2 to 6°C for all the resolutions examined (Figure 4). This is consistent with the finding that "thermodynamics" could be an important causative factor for extreme precipitation in mid-latitudes as Emori and Brown (2005) have reported.

The updraft velocities that accompany precipitation extremes have strong sensitivity to horizontal resolution at the original model grids (not shown here). After averaged to 5-degree grid (blue line in Figure 4), there is a strong increase of updraft from T42 to T170, but the difference between T170 and T340 is small. The anomalies in updraft magnitude have almost the same meridional structure as the extreme precipitation. In each specific horizontal resolution, the zonal-mean updraft anomalies are

also highly anti-correlated ($r < -0.8$) with the extreme precipitation. The strong coupling of updraft and extreme precipitation suggest that enhanced updraft velocity could be an important factor in the resolution dependency of extreme precipitation and also the primary physical driver for extreme precipitation, as suggested by other studies (e.g. O'Gorman and Schneider (2009). However the release of latent heat from extreme precipitation could have also contributed the strong upward motion, as the dynamics are unlikely to create those strong motions in the absence of other processes. If this is the case, as discussed above that the maximum latent heating appears near 500-600 hPa level over tropics (Boyle and Klein, 2010), the lack of strong positive temperature anomalies associated with extreme precipitation at the equator in Figure 4 is likely due to the low level we choose in this study.

4. Conclusions and discussions

In this study we investigate the impact of horizontal resolution on the simulation of precipitation extremes in a climate model using an aqua-planet version of Eulerian spectral Community Atmosphere Model CAM3 (Collins et al., 2004). Ten experiments have been performed at four horizontal-resolutions (T42, T85, T170, and T340) and various time steps at or below their dynamical stability at each resolution. We consider the effect of horizontal resolution on the large scales only by averaging the simulation data to a 5-degree grid for all the analyses presented here.

The study shows that the precipitation extremes do not converge across horizontal resolutions at the same time step. The horizontal resolution has much stronger impact on precipitation extremes compared with mean precipitation, especially in tropics. Under the

standard climate model runs at different resolutions, the increasing resolution requires shorter time steps in accordance with the CFL criterion. Since both these two changes lead to increase of precipitation extremes, the differences in the statistics of precipitation extremes are more pronounced for standard climate model runs. The projection of precipitation extremes depends on the choice of resolution and time step, and the metrics used to improve the realism of mean precipitation may be inadequate to insure either the fidelity or the resolution invariance of extremes in climate models. The parameterizations of extremes need to be improved so that retrospective simulations of these phenomena converge to the observational record at sufficiently high resolution.

The divergence of large extreme precipitation is primarily due to the parameterization of prognostic large-scale precipitation. During the extreme events, the large-scale precipitation greatly increases but the convection precipitation decreases with increasing resolution. The trend for large-scale precipitation is similar but weaker than that for mean precipitation. Boyle and Klein (2010) also reported the increase large-scale to convective precipitation ratio with increasing resolution in real-world simulations with CAM (version 4). They attributed this change to reduced evaporation of large-scale precipitation in the lower troposphere rather than increased condensation in the upper troposphere as the resolution of the model grids is refined (Duffy et al. 2003).

In tropical regions, the convective precipitation rarely produces any precipitation greater than 30 mm/day on the 5° grid, partially due to the spatial smoothing, and it contributes little to the extreme precipitation at the tails of the distribution. Durman et al. (2001) also identified a similar issue with a low-resolution HadCM2 GCM, which simulated poorly the European daily precipitation events exceeding 30 mm/day. We

showed that more total precipitation is explicitly resolved with increased resolution in aqua-planet runs. As many large-scale processes, such as large-scale condensation, will benefit from the resolved detail in high-resolution runs, the increased total precipitation is likely treated as large-scale precipitation in the model. The convective precipitation, however, may still remain unresolved in the even the highest horizontal resolution runs used (T340: ~0.35°) used in this study.

This study also presents information for a better understanding of the mechanisms that trigger the precipitation extremes under the aqua-planet framework. The modeled near-surface temperature and vertical velocity ω, representing the "dynamic" and "thermodynamic" effects respectively, were studied and we found each parameter appears to be important at different latitudes. The extreme events are usually accompanied by near-surface warming in mid to high latitudes for all the resolutions, and the thermodynamics likely to play an important role in triggering extreme precipitation in this region, as reported previously by Emori and Brown (2005). In the tropics, extreme precipitation shows strong coupling with perturbations in updraft velocities. However we cannot ascribe cause and effect here because the dynamics requires a forcing such as provided by the release of latent heat to create the extreme updrafts but the extreme precipitation requires strong moisture convergence associated with the updraft to provide the moisture.

References:

Alexander, L. V., Zhang, X., Peterson, T. C., Caesar, J., Gleason, B. and co-authors. 2006. Global observed changes in daily climate extremes of temperature and precipitation, *J. Geophys. Res., 111*, D05109, doi:10.1029/2005JD006290.

Boyle, J. and Klein, S. A. 2010. Impact of horizontal resolution on climate model forecasts of tropical precipitation and diabatic heating for the TWP-ICE period, *J. Geophys. Res., 115*, D23113, doi:10.1029/2010JD014262.

Chen, C. T. and Knutson, T. 2008. On the verification and comparison of extreme rainfall indices from climate models, *J. Climate, 21*, 1605–1621.

Christensen, J. H. and Christensen O. B. 2003. Severe summertime flooding in Europe, *Nature, 421*, 805–806.

Collins, W. D., Rasch, P. J., Boville, B. A., Hack, J. J., McCaa, J. R., and co-authors. 2004. Description of the NCAR Community Atmosphere Model (CAM3), *Tech. Note NCAR-TN-464+STR*, Natl. Cent. for Atmos. Res., Boulder, Colo.

Courant, R., Friedrichs, K. and Lewy, H. 1967. On the partial difference equations of mathematical physics. *IBM Journal (March)*, 215–234.

Duffy, P. B., Govindasamy, B., Iorio, J. P., Milovich, J., Sperber K. R. and co-authors. 2003. High-resolution simulations of global climate, Part 1: present climate, *Climate Dynamics, 21*, 317-390.

Durman C. F., Gregory, J. M., Hassell, D. C., Jones, R. G. and Murphy J. M. 2001. Comparison of extreme European daily precipitation simulated by a global and a regional climate model for present and future climates, *Quarterly Journal of the Royal Meteorological Society, 127,* 1005–1015, doi: 10.1002/qj.49712757316.

Emori, S., and Brown, S. J. 2005. Dynamic and thermodynamic changes in mean and extreme precipitation under changed climate. *Geophys. Res. Lett., 32*, L17706, doi:10.1029/2005GL023272.

Frich, P., Alexander, L. V., Della-Marta, P., Gleason, B., Haylock, M. and co-authors. 2002. Observed coherent changes in climatic extremes during the second half of the twentieth century, *Clim. Res., 19*, 193–212.

Ghan S, Bian, X., Hunt A. and Coleman A. 2002. The thermodynamic influence of subgrid orography in a global climate model, *Climate Dyn. 20* (1), 31-44, doi: 10.1007/s00382-002-0257-5.

Giorgi, F. and Avissar R. 1997. Representation of heterogeneity effects in Earth system modeling: Experience from land surface modeling, *Rev. Geophys., 35*(4), 413–437, doi:10.1029/97RG01754.

Hack, J. J., Caron, J. M., Danabasoglu, G., Oleson, K. W., Bitz, C. M. and Truesdale J. E. 2006. CCSM-CAM3 climate simulation sensitivity to changes in horizontal resolution, *J. Clim., 19*, 2267–2289.

Kharin, V. V., Zwiers, F. W., Zhang, X. and Hegerl G. C. 2007. Changes in temperature and precipitation extremes in the IPCC ensemble of global coupled model simulations. *J. Climate, 20*, 1419–1444.

Lau, N.-C. and Ploshay J. J. 2009. Simulation of synoptic- and subsynoptic-scale phenomena associated with the East Asian summer monsoon using a high-resolution CCM, *Monthly Weather Review, 137*(1), 137-160.

Neale R. B., and Hoskins B. J. 2000. A standard test for AGCMs including their physical parametrizations: I: the proposal, *Atmos. Sci. Lett., 1*(2), 101–107,

doi: 10.1006/asle.2000.0022

O'Gorman, P. A., and Schneider, T. 2009. Scaling of precipitation extremes over a wide range of climates simulated with an idealized GCM, *J. Clim., 22*, 5676–5685.

Pall, P., Allen, M. R. and Stone, D. A. 2007. Testing the Clausius- Clapeyron constraint on changes in extreme precipitation under CO2 warming, *Clim. Dyn., 28*, 351–363, doi:10.1007/s00382-006-0180-2.

Parry, M.L., Canziani, O.F., Palutikof J.P. and co-authors. 2007. Technical Summary. *Climate Change 2007: Impacts, Adaptation and Vulnerability. Contribution of Working Group II to the Fourth Assessment Report of the Intergovernmental Panel on Climate Change*, M.L. Parry, O.F. Canziani, J.P. Palutikof, P.J. van der Linden and C.E. Hanson, Eds., Cambridge University Press, Cambridge, UK, 23-78.

Pope, V. D. and Stratton R. A. 2002. The processes governing horizontal resolution sensitivity in a climate model, *Climate Dynamics, 19*, 211-236.

Randall, D. A., Wood, R. A., Bony, S., Colman, R., Fichefet, T. and co-authors. 2007. Climate Models and Their Evaluation. In: *Climate Change 2007: The Physical Science Basis. Contribution of Working Group I to the Fourth Assessment Report of the Intergovernmental Panel on Climate Change* [Solomon, S., D. Qin, M. Manning, Z. Chen, M. Marquis, K.B. Avery, M. Tignor and H.L. Miller (eds.)]. Cambridge University Press, Cambridge, United Kingdom and New York, NY, USA.

Rasch, P. J., Stevens, M. J., Ricciardulli, L., Dai, A., Negri, A. and co-authors. 2006. A Characterization of Tropical Transient Activity in the CAM3 Atmospheric Hydrologic Cycle. *J. Climate, 19*, 2222–2242. doi: 10.1175/JCLI3752.1.

Schneider, T., and O'Gorman, P. A. 2007. Precipitation and its extremes in changed

climates. Extreme Events: Proc. *'Aha Huliko'a Hawaiian Winter Workshop*, Honolulu, HI, University of Hawaii at Manoa, 61–66.

Schumacher, C. and Houze R. A. 2003. Stratiform rain in the tropics as seen by the TRMM precipitation radar, J. Clim., 16(11), 1739–1756.

Sun, Y., Solomon, S., Dai, A. and Portmann R. W. 2006. How often will it rain? *J. Climate, 20*, 4801–4818.

Trenberth, K.E., Jones, P. D., Ambenje, P., Bojariu, R. and Easterling, D. and co-authors. 2007. Observations: Surface and Atmospheric Climate Change. In: *Climate Change 2007: The Physical Science Basis*. Contribution of Working Group I to the Fourth Assessment Report of the Intergovernmental Panel on Climate Change [Solomon, S., D. Qin, M. Manning, Z. Chen, M. Marquis, K.B. Averyt, M. Tignor and H.L. Miller (eds.)]. Cambridge University Press, Cambridge, United Kingdom and New York, NY, USA.

Williamson. D. L. 2008, Convergence of aqua-planet simulations with increasing resolution in the Community Atmospheric Model, Version 3. *Tellus, 60A*, 848–862.

Wehner M. F., Bala, G., Duffy, P., Mirin, A. A. and Romano R. 2010. Towards Direct Simulation of Future Tropical Cyclone Statistics in a High-Resolution Global Atmospheric Model," *Advances in Meteorology, vol. 2010*, Article ID 915303, 13 pages, 2010. doi:10.1155/2010/915303.

Wilcox, E. M. and Donner L. J. 2007. The frequency of extreme rain events in satellite rain-rate estimates and an atmospheric general circulation model. *J. Climate, 20*, 53–69.

Acknowledgments. This work was supported by the Director, Office of Science, Office of Biological and Environmental Research, Climate Change Research Division, of the U.S. Department of Energy under Contract No. DE-AC02-05CH11231. Williamson and Olson were partially supported by the Office of Science (BER), U.S. Department of Energy, Cooperative Agreement No. DE-FC02-97ER62402. The National Center for Atmospheric Research is sponsored by the National Science Foundation.

Figures:

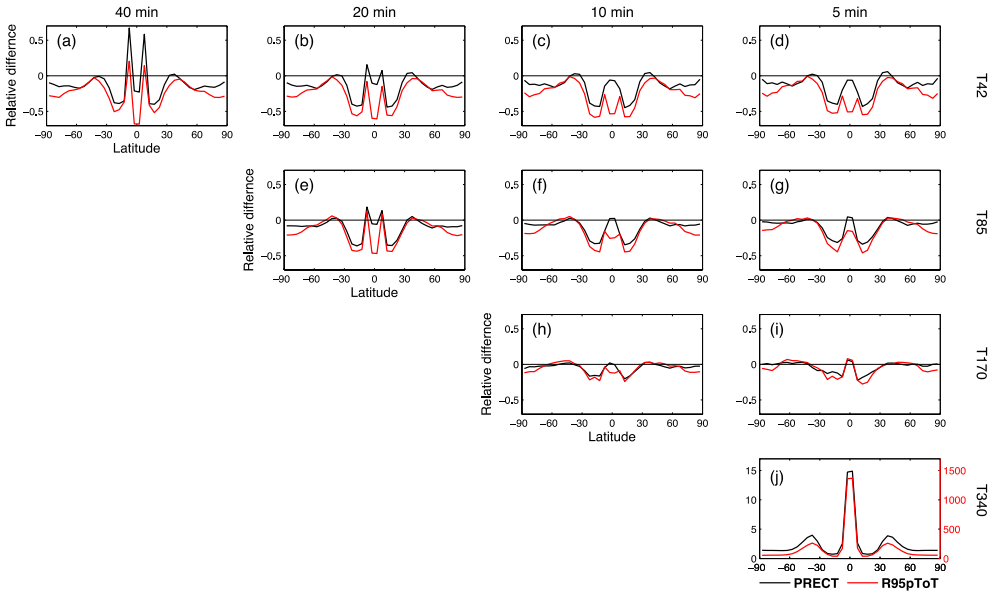

Figure 1. The relative difference of time-averaged, zonal-averaged daily total precipitation (PRECT) in black and precipitation extremes (R95pTOT) in red, with respect to results from a T340 reference simulation run with a 5 minute physics time step. The relative difference is calculated by (Txx–T340)/T340. Panel j shows the absolute amounts of daily precipitation (mm/day; black axis) and R95pTOT precipitation extreme (mm/year; red axis) in the T340 reference case.

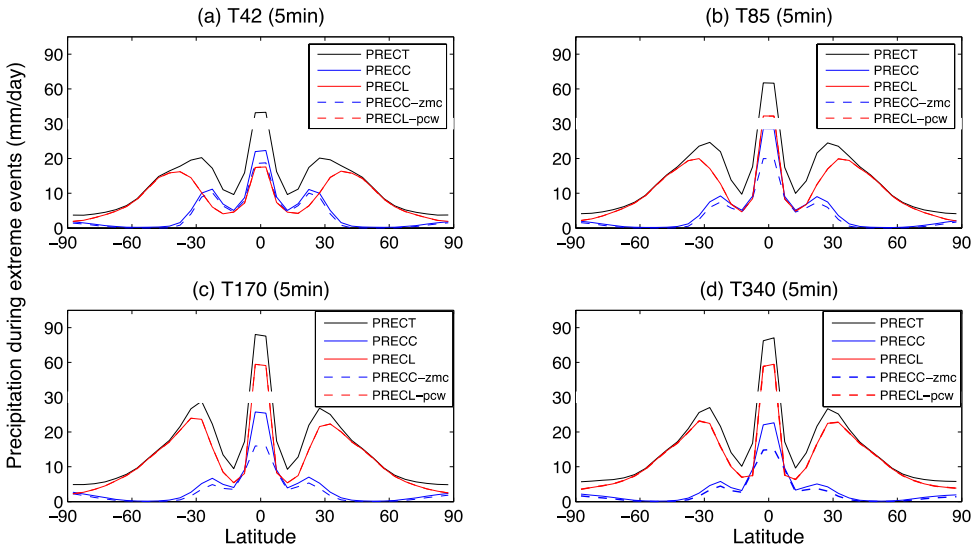

Figure 2. Different components of the time-averaged, zonal-averaged daily precipitation extremes (mm/day) during 95% percentile extreme events from simulations at four different spatial resolutions and a fixed 5-minute timestep. The dashed red line falls under the solid red line.

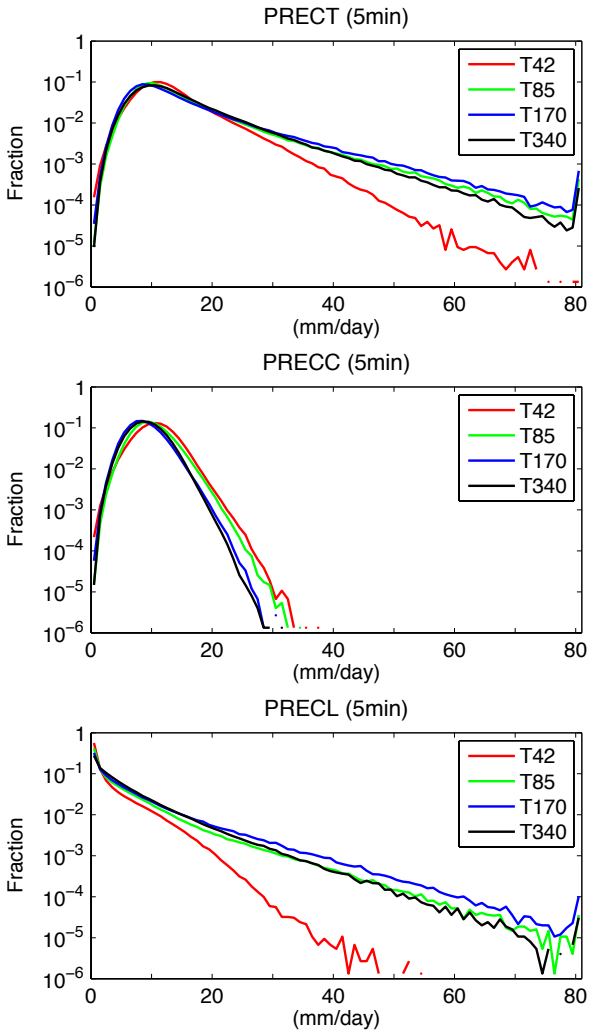

Figure 3: Probability distributions of daily precipitation in the equatorial zone from 5° S to 5° N aggregated in 1mm/day bins from 0 to 80 mm/day. Precipitation larger than 80 mm/day is treated as one bin. Distributions of total precipitation (PRECT), convective precipitation (PRECC), and large-scale precipitation (PRECL) are shown for simulations at four horizontal resolutions and a fixed 5-minute timestep.

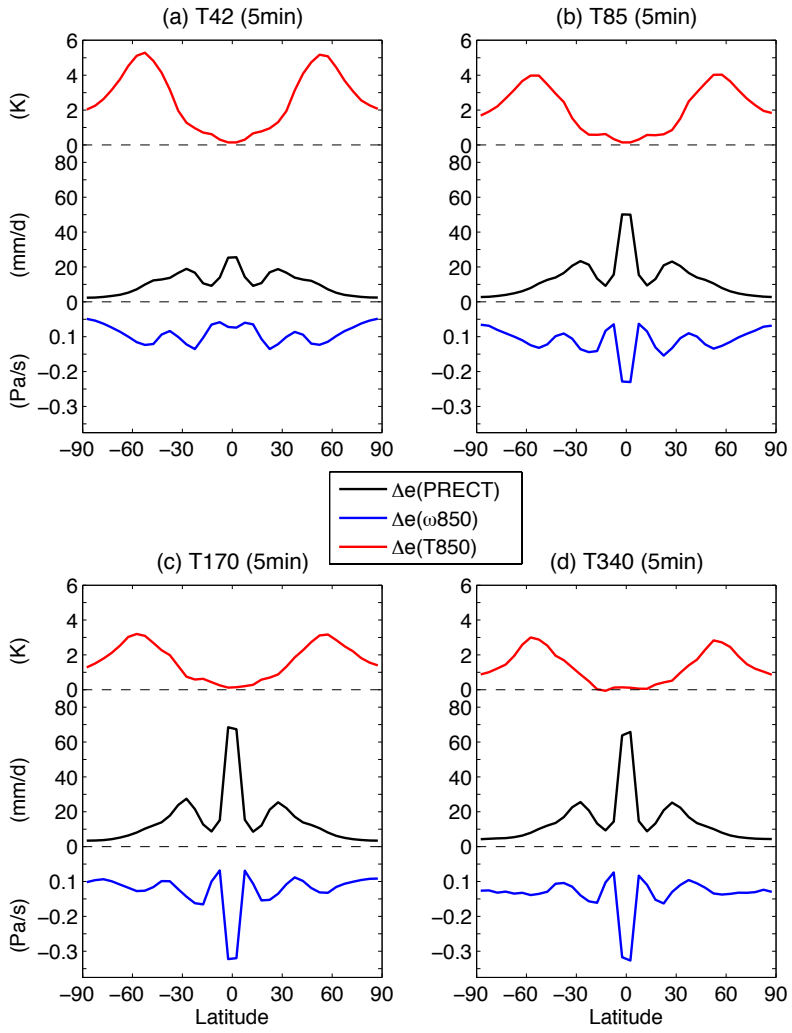

Figure 4. Zonal-mean anomalies of extreme precipitation (black line), 850 hPa vertical velocity ω (blue line) and 850 hPa temperature (red line) as functions of horizontal resolution. The anomalies are calculated by subtracting the climatological mean values from mean values of the fields sampled only during extreme precipitation events, and the fields have been averaged to 5-degree grids before the calculation. The extreme precipitation is larger than 95th percentile daily

precipitation used to calculate R95pTOT. The vertical velocity ω (Pa/s) and temperature (K) correspond to the 850 hPa pressure surface. Negative ω indicates updraft.